Improving Oxygen Barrier Properties of Poly(ethylene terephthalate) by Incorporating Isophthalate. II. Effect of Crystallization

Y. S. Hu, A. Hiltner, E. Baer

Department of Macromolecular Science and Engineering, Center for Applied Polymer Research, Case Western Reserve University, Cleveland, Ohio 44106

Received 4 January 2005; accepted 28 February 2005
DOI 10.1002/app.22214
Published online in Wiley InterScience (www.interscience.wiley.com).

ABSTRACT: The present study examined crystallization of poly(ethylene terephthalate) (PET) and a series of random and blocky copolymers in which up to 30% of the terephthalate was replaced with isophthalate. Isothermal crystallization kinetics and direct observation of the spherulitic morphology revealed that the blocky copolymers crystallized more rapidly than PET, at least in part, as the result of enhanced spherulite nucleation. The statistical copolymers with 10 and 20% isophthalate achieved almost the same level of crystallinity as that of the blocky copolymers. The statistical copolymers with 10% isophthalate crystallized almost as fast as PET, although the statistical copolymer with 20% isophthalate crystallized much more slowly. Crystallization substantially reduced the oxygen permeability. Analysis of oxygen-transport parameters in terms of a two-phase structural model that considered a dispersion of lower-permeability spherulites in an amorphous matrix of higher permeability revealed that dedensification of the PET interlamellar amorphous regions was responsible for the unexpectedly high oxygen solubility of crystallized PET. In contrast, copolymerization with isophthalate prevented dedensification of the interlamellar amorphous regions. As a result, crystallization was more effective in reducing the oxygen permeability. It was speculated that segregation of kinked isophthalate units to the amorphous regions of the spherulite relieved constraint on the interlamellar amorphous chain segments. © 2005 Wiley Periodicals, Inc. J Appl Polym Sci 98: 1629–1642, 2005

Key words: poly(ethylene terephthalate) (PET); crystallization; blends; barrier; copolymers

INTRODUCTION

One approach to improving gas barrier properties of poly(ethylene terephthalate) (PET) focuses on copolymerization with a higher barrier component. A companion study describes a series of random and blocky copolymers in which up to 30% of the terephthalate in PET is replaced with isophthalate.[1] The blocky copolymers exhibit a single glass transition with the same composition dependency as the glass transition of random copolymers, which indicates that PET and poly(ethylene isophthalate) (PEI) blocks are miscible in the glass. As a result, blocky and random copolymers exhibit essentially the same properties in the glassy state. However, blocky copolymers with up to 30% isophthalate are readily oriented. In contrast, statistical incorporation of more than 10% isophthalate adversely affects orientation.

The previous study also found that the nature of isophthalate distribution strongly affects crystallization from the glass.[1] Blocky copolymers with up to 30% isophthalate crystallize rapidly to achieve a total crystallinity close to that of PET. In contrast, statistical distribution of isophthalate units significantly retards cold crystallization to the extent that random copolymers with more than 10% isophthalate do not crystallize when heated at a rate of 10°C min^{-1}.

The present article further compares the crystallization habits of random and blocky copolymers by examining isothermal crystallization kinetics, crystalline morphology, and oxygen-transport characteristics. In addition to being an important performance property, oxygen permeability becomes a powerful structural probe when separated into its thermodynamic and kinetic components of gas solubility and gas diffusivity.[2] Morphological observations are compared against a structural model of oxygen transport that considers a dispersion of lower-permeability spherulites in an amorphous matrix of higher permeability.[3] In particular, the model reveals the effects of crystallization on amorphous phase properties such as density and permeability. Of specific interest is dedensification of the interlamellar amorphous regions, which compromises the barrier enhancement that can be achieved by crystallization of PET.[4–6] The possibility

Correspondence to: A. Hiltner (pah6@case.edu).
Contract grant sponsor: KoSa.

is tested that segregation of noncrystallizable isophthalate units into the amorphous regions relieves constraints on interlamellar amorphous chain segments and thereby prevents amorphous phase densification.

EXPERIMENTAL

Synthesis and characterization of PET, PEI, and statistical copolymers of ethylene terephthalate with 10, 20, and 30% ethylene isophthalate (PET-*co*-10I, PET-*co*-20I, and PET-*co*-30I) were described previously.[1] The PET was melt-blended with 10, 20, and 30% PEI (PET-*b*-10I, PET-*b*-20I, and PET-*b*-30I). As demonstrated by nuclear magnetic resonance (NMR) spectroscopy, some level of transesterification during melt processing resulted in materials that were better described as blocky copolymers than as physical blends.[1]

The pellets were dried in vacuum and 0.2 mm thick films were compression molded at 270°C and quenched in cold water. The clear films, used to study crystallization kinetics, were also used to prepare specimens for atomic force microscopy (AFM), X-ray diffraction (XRD), and oxygen-transport measurements. Cold-crystallized barrier specimens were prepared for PET, PET-*co*-10I, PET-*b*-10I, PET-*b*-20I, and PET-*b*-30I by annealing amorphous films in an oven at 120°C and quenching into cold water. Films were crystallized for various periods of time from 4 min to 8 h to obtain specimens that differed in the amount of crystallinity.

Isothermal crystallization was performed with a DSC-7 apparatus (Perkin–Elmer, Shelton, CT), calibrated with indium and tin standards. Specimens were heated at 100°C min^{-1} to the crystallization temperature. Isothermal crystallization was performed between 110 and 130°C for PET, PET-*b*-10I, PET-*b*-20I, and PET-*b*-30I. For random copolymers, isothermal crystallization was conducted in the same way except that the crystallization temperatures ranged from 110 to 150°C for PET-*co*-10I and from 140 to 170°C for PET-*co*-20I. The detailed procedure was described previously.[7]

Density was measured with a density gradient column constructed from an aqueous solution of calcium nitrate in accordance with ASTM-D 1505 Method B. The column was calibrated with glass floats of known density. Small pieces of film ($\sim$ 25 mm^2) were placed in the column and allowed to equilibrate for 30 min before the measurements were taken. Wide-angle X-ray diffraction (WAXD) was performed at ambient temperature in the transmission mode in a Philips diffractometer (Philips, Eindhoven, The Netherlands) with Cu–$K_{\alpha 1}$ radiation and slit angle of 0.5°.

For AFM measurements, specimens were sectioned with an Ultramicrotome (MT6000-XL; RMC, Tucson, AZ) and etched. Various methods for selective etching of aromatic polyesters were tried.[7–11] The best results were obtained by etching at ambient temperature for 15 min with a solution of 2 mg potassium permanganate mL^{-1} of a concentrated sulfuric acid, orthophosphoric acid (85%), water mixture. The composition of the concentrated sulfuric acid, orthophosphoric acid (85%), water mixture (v/v/v) was 3 : 1 : 1.9–2.0 for PET, 3 : 1 : 2.1 for PET-*b*-10I, 3 : 1 : 2.2 for PET-*b*-20I, 3 : 1 : 2.3 for PET-*b*-30I, and 3 : 1 : 2.5 for PET-*co*-10I. The etched surfaces were examined in air at ambient conditions using the Nanoscope IIIa MultiMode head from Digital Instruments (Santa Barbara, CA) in the tapping mode. Phase and height images were recorded simultaneously.

Oxygen flux $J(t)$ at 0% relative humidity, 1 atm pressure, and 23°C was measured with an OX-TRAN 2/20 apparatus (MOCON, Minneapolis, MN). Additional experiments were carried out at various temperatures between 10 and 40°C. Diffusivity D and permeability P were obtained by fitting the nonsteady-state flux–time curve to the solution to Fick's second law with appropriate boundary conditions.[4]

RESULTS

Crystallization kinetics

Thermal properties of the quenched, compression-molded films determined with scanning methods (DSC and DMTA) are summarized in Table I. A single glass transition with the same composition dependency for random and blocky copolymers indicated that PET and PEI blocks were miscible in the glass. As a result, random and blocky copolymers exhibited similar glassy state properties. However, isophthalate distribution strongly affected cold crystallization from the glass, as evident in peak crystallization and melting temperatures and the corresponding enthalpies. Random distribution of isophthalate units significantly retarded cold crystallization to the extent that PET-*co*-20I crystallized only slightly and PET-*co*-30I did not crystallize when heated at a rate of 10°C min^{-1}. In contrast, blocky copolymers with up to 30% isophthalate cold crystallized rapidly to achieve a total crystallinity close to that of PET. The enthalpies of cold crystallization and melting did not reduce in proportion to the amount of terephthalate, which suggested that PEI blocks cocrystallized to some extent.[12,13]

Rapid crystallization of PET and the blocky copolymers limited the temperature range for isothermal cold-crystallization studies from 110 to 130°C. Slower crystallization of the random copolymers permitted investigation of the cold-crystallization kinetics over a broader temperature range from 110 to 150°C for PET-*co*-10I and from 140 to 170°C for PET-*co*-20I. Typical isothermal DSC curves in Figure 1 show exothermic heat flow at 120°C for cold crystallization of PET, PET-*co*-10I, and the three blocky copolymers. The rel-

TABLE I
Thermal Properties of Quenched Films

	First heating					Cooling	
Polymer	T_g (°C)	T_{cc} (°C)	ΔH_{cc} (J g^{-1})	T_m (°C)	ΔH_m (J g^{-1})	T_c (°C)	ΔH_c (J g^{-1})
PET	76	140	34	246	35	186	35
PET-*co*-10I	72	151	31	233	32	180	32
PET-*co*-20I	68	171	1.4	205	1.2	137	4
PET-*co*-30I	66	—	—	—	—	—	—
PET-*b*-10I	72	134	33	245	34	193	35
PET-*b*-20I	69	134	32	243	34	201	35
PET-*b*-30I	65	139	28	240	29	191	31
PEI	55	166	3.5	235	3.5	—	—

ative crystallinity X_t, defined as the ratio of crystallinity at time t to crystallinity at t_∞, is given as

$$X_t = \frac{\int_0^t (dH/dt)dt}{\int_0^\infty (dH/dt)dt} = \frac{\Delta H_t}{\Delta H_\infty} \quad (1)$$

where dH/dt is the rate of heat evolution, ΔH_t is the total heat evolved at time t, and ΔH_∞ is the total heat evolved as time approaches infinity.

Plots of relative crystallinity as a function of time showed the sigmoidal shape typical of isothermal polymer crystallization (Fig. 2). At 120°C, PET-*b*-10I crystallized the most rapidly; the crystallization rate decreased, approaching that of PET, as the isophthalate content of the blocky copolymer increased. A slightly higher crystallization rate of PET-*b*-20I compared to that of PET was observed previously.[14] The random copolymer PET-*co*-10I crystallized much more slowly than PET and crystallization of PET-*co*-20I was too slow at this temperature to be measured readily. From the isotherms, the half-time of crystallization $t_{1/2}$, defined as the time required to reach $X_t = 0.5$, was determined (Table II). The values of $t_{1/2}$ for PET were in agreement with data reported in the literature.[15,16]

Typically, $t_{1/2}$ represents the overall crystallization rate and is governed by the rates of nucleation and growth. The combined effects produce a maximum in the crystallization rate, or a minimum in $t_{1/2}$, at a temperature between the melting point and the glass-transition temperature, thereby giving rise to the so-called bell curve of isothermal crystallization. Because of the high rate of cold crystallization, only the low-temperature side of the bell curve was accessible for PET, PET-*co*-10I, and the blocky copolymers. For these polymers, $t_{1/2}$ was <1 min at temperatures well below the anticipated minimum value. Only PET-*co*-10I crystallized slowly enough for the DSC method to access the entire curve (Fig. 3). The crystallization rate passed through a broad maximum (minimum in $t_{1/2}$) at about 155°C with $t_{1/2}$ of about 6.5 min.

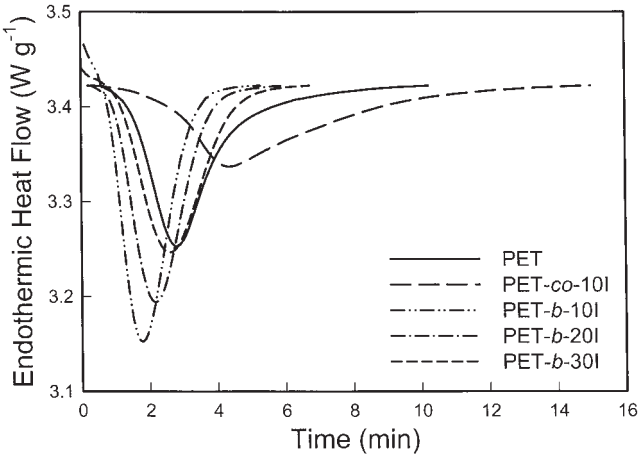

Figure 1 Isothermal DSC traces for cold crystallization at 120°C.

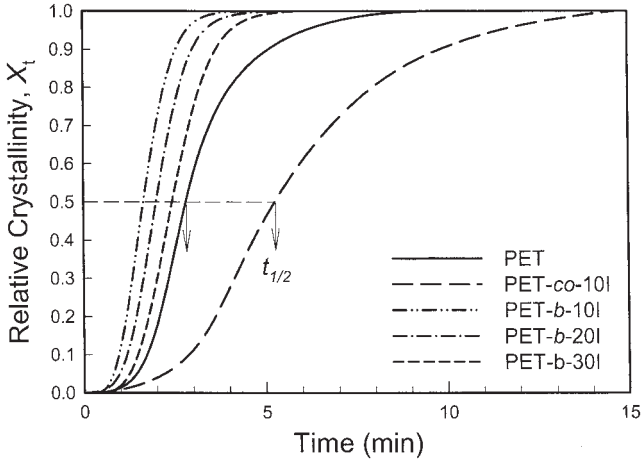

Figure 2 Relative crystallinity as a function of time obtained from DSC traces in Figure 1.

TABLE II
Parameters Describing Isothermal Crystallization Kinetics

Polymer	Temperature (°C)	$t_{1/2}$ (min)	n	ΔH_∞ (J g^{-1})	t_∞ (min)
PET	115	6.3	3.4	24	13
	120	2.8	3.8	26	8.6
	125	1.5	3.7	24	6.0
	130	0.8	3.6	29	3.2
PET-*co*-10I	115	8.9	3.7	24	25
	120	5.5	3.8	25	20
	130	1.7	3.7	25	11
	140	0.9	3.5	26	8.1
	150	0.8	3.8	26	3.8
PET-*co*-20I	140	9.4	3.2	23	28
	150	6.9	2.6	24	22
	160	6.8	3.1	25	18
	170	8.0	2.7	27	23
PET-*b*-10I	110	6.6	3.2	25	17
	115	3.3	3.4	26	8.6
	120	1.7	3.4	26	6.6
	125	0.8	3.4	28	2.6
	130	0.5	3.2	29	1.9
PET-*b*-20I	110	7.0	3.7	25	18
	115	4.1	3.9	25	9.9
	120	2.1	3.7	24	6.0
	130	0.7	3.4	27	2.6
PET-*b*-30I	115	6.1	3.7	24	11
	120	2.5	3.6	22	7.1
	130	0.9	3.5	25	3.6

Although isothermal crystallization of PET-*co*-20I was very slow, the amount of crystallinity achieved as indicated by ΔH_∞ was comparable with that of PET and the other copolymers (Table II). A DSC thermogram of the isothermally crystallized specimen, obtained with a heating rate of 10°C min^{-1}, confirmed the high level of crystallinity, $\Delta H_m \approx 25$ J g^{-1}. To eliminate the possibility that high crystallinity resulted from blockiness imparted by transesterification during thermal crystallization, the specimen was subsequently quenched to the glass and reheated. The resulting thermogram was the same as that of a specimen that had not experienced isothermal crystallization with a small cold-crystallization exotherm, $\Delta H_{cc} \approx 5$ J g^{-1}, just before melting. It appeared that slow crystallization to a substantial level of crystallinity was an intrinsic characteristic of PET-*co*-20I. This characteristic was also manifest as strain-induced crystallization if the draw rate was low enough.[1]

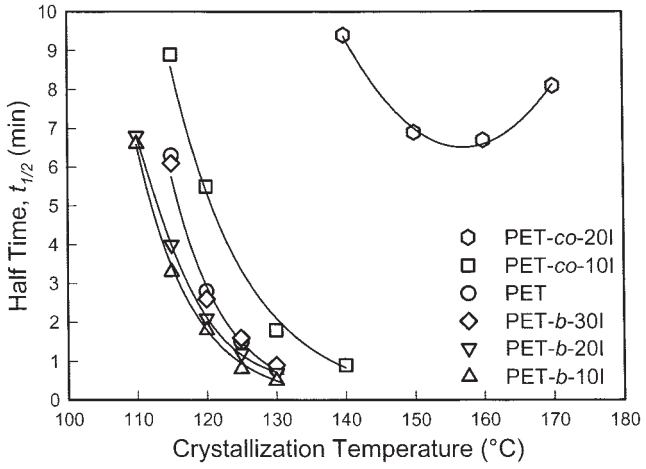

Figure 3 Half-time for crystallization of PET and copolymers.

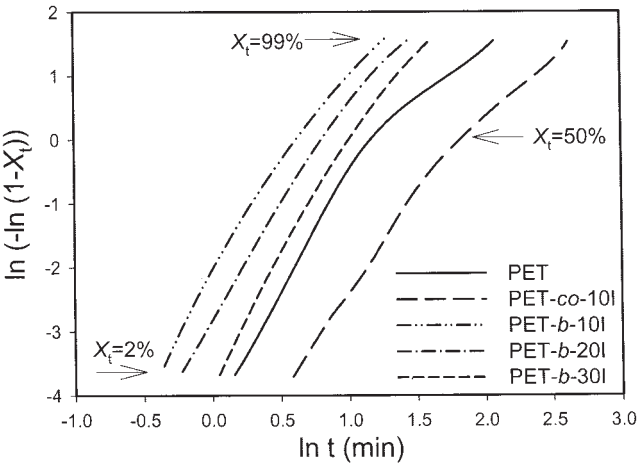

Figure 4 Relative crystallinity from Figure 2 plotted according to the Avrami relationship [eq. (3)].

Following the classic Avrami equation

$$1 - X_t = \exp(-kt^n) \tag{2}$$

where k is the crystallization rate constant and n is the Avrami exponent describing the crystal growth geometry and nucleation mechanism, and the data in Figure 2 were plotted according to

$$\ln[-\ln(1 - X_t)] = n \ln t + \ln k \tag{3}$$

to obtain the Avrami parameters n and k.[17] Avrami plots for PET and PET-*co*-10I exhibited an initial linear region with deviation at longer times because of spherulite impingement (Fig. 4). Avrami plots for the blocky copolymers did not show such a distinct deviation from linearity in the later stages of crystallization, which is similar to a previous finding.[14] For consistency, the Avrami exponent n and the rate constant k were calculated from the linear region of primary crystallization between $X_t = 0.01$ and $X_t = 0.50$. The results are summarized in Table II. In most cases, the exponent n was 3–4, corresponding to spherulitic growth with heterogeneous nucleation. An exponent n of 3 for PET-*co*-20I could be attributed to imperfect crystals and low dimension of crystal growth.[18]

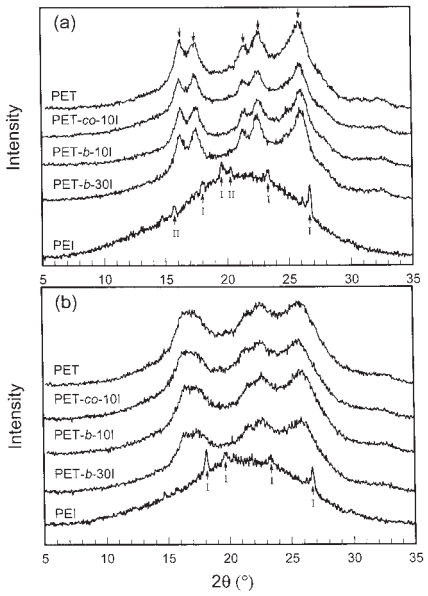

Figure 5 WAXD patterns of crystalline films: (a) cold crystallized at 200°C for 2 h; and (b) cold crystallized at 120°C for 4 h (PET, PET-*b*-10I and PET-*b*-30I) or for 8 h (PET-*co*-10I and PEI).

Crystalline morphology

WAXD patterns of films isothermally crystallized at 200 and 120°C are shown in Figure 5. All the diffraction patterns showed crystalline peaks superimposed onto a broad amorphous reflection. The triclinic crystal structure of PET is well known. The main diffraction peaks for annealed PET film typically appear at 2θ of 16.5° ($0\bar{1}1$), 17.8° (010), 21.8° ($\bar{1}11$), 23.0° ($1\bar{1}0$), and 26.2° (100).[19] All of these were present in the WAXD pattern of crystallized PET films, although they were not well resolved in films crystallized at 120°C. The diffraction patterns of PET-*co*-10I and the blocky copolymers closely resembled the PET diffraction pattern.

Two crystal forms have been described for PEI, types I and II, depending on thermal history.[20–22] The diffraction peaks at 18.2, 19.8, 23.4, and 26.7° indicated cold-crystallized PEI took primarily the type I form. Crystallization at 200 and 120°C gave essentially the same diffraction pattern. Absence of characteristic PEI reflections from WAXD patterns of the blocky copolymers demonstrated that the PEI blocks did not crystallize separately with the PEI unit cell.

The possibility exists that isophthalate units are incorporated into the PET crystal to some extent. Although the diffraction patterns of crystalline PET and PEI differ substantially, it has been suggested that isophthalate units can enter into the unit cell of PET by slight rotation of the CH_2 bonds in the methylene segments.[23] Inclusion of isophthalate in the PET unit cell was demonstrated for random copolymers with more than 12% isophthalate.[24–26] Some amount of cocrystallization could account for the disproportionately high heat of melting of blocky copolymers, as well as the high crystallinity achieved by isothermal crystallization of PET-*co*-20I. For this reason, the crystal density ρ_c of the copolymers is taken as 1.476 g cm^{-3}, which is considered as an intrinsic characteristic of the defective crystalline PET phase.[27]

To obtain specimens that differed in the amount of crystallinity, amorphous films of PET, PET-*co*-10I, and PET-*b*-10I were held at 120°C for various periods of time before crystallization was arrested by quenching into cold water. The increase in crystallinity, expressed as density, followed the typical sigmoidal dependency on isothermal crystallization time, as shown in Figure 6. The region of rapidly increasing density corresponded to increasing volume fraction spherulites by the processes of nucleation and growth. Secondary crystallization accounted for a small density increase at longer times, after the spherulites were space filling.

A 50-μm AFM height image of a PET film, crystallized for 20 min with $\phi_c = 0.17$, displayed isolated or partially impinged compact spherulites dispersed in an amorphous matrix [Fig. 7(a)]. The spherulites were on a size scale of 10 μm. After 4 h at 120°C, space-filling, impinging spherulites with sharp boundaries characterized the completely crystallized film [Fig. 7(b)]. The spherulite diameter was about 20 μm. A 3-μm phase image [Fig. 7(c)], taken from a spherulite arm in Figure 7(b), showed short, densely packed lamellae. Lamellar thickness measured from the phase image was about 40–50 nm. Such granular lamellae were reported for PET crystallized from the glassy state at 100–150°C.[28]

The cold-crystallization habit of PET-*co*-10I closely resembled that of PET. A 50-μm AFM height image of a PET-*co*-10I film, crystallized for 1 h at 120°C with ϕ_c

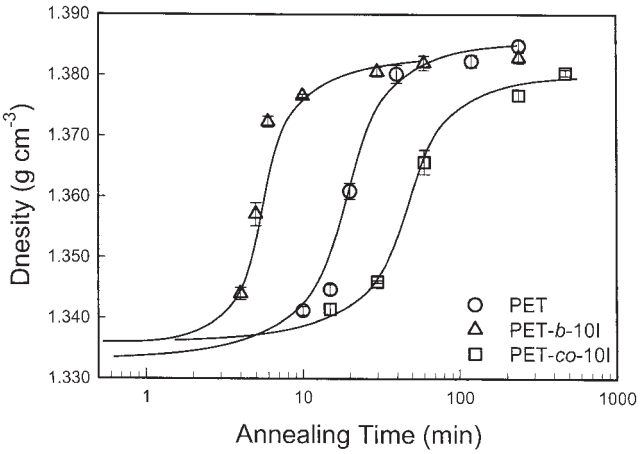

Figure 6 Crystallinity measured as density as a function of crystallization time at 120°C.

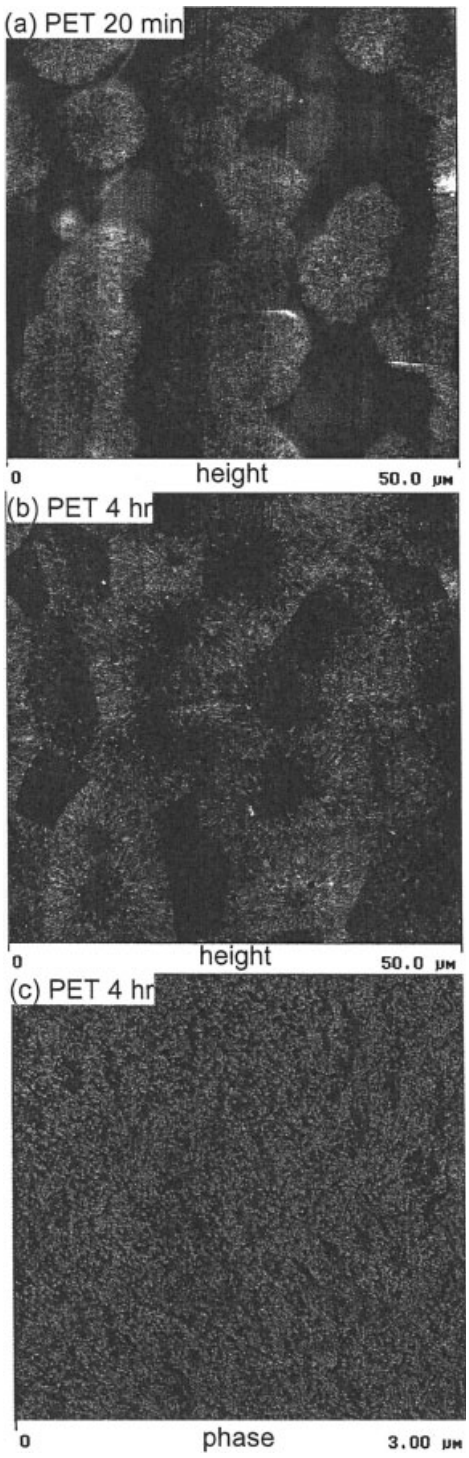

Figure 7 AFM images of PET cold crystallized at 120°C: (a) height image after crystallization for 20 min; (b) height image after crystallization for 4 h; and (c) high-resolution phase image from a spherulite arm in (b).

= 0.18, displayed well-defined isolated or partially impinged spherulites [Fig. 8(a)]. The spherulites were on a size scale of 5 μm. After crystallization for 8 h, the morphology consisted of space-filling spherulites with sharp boundaries [Fig. 8(b)]. The spherulite size and lamellar texture [Fig. 8(c)] were about the same as seen in completely crystallized PET [Fig. 7(b, c)].

A high density of very small embryonic spherulites was seen in a 10-μm AFM height image of PET-*b*-10I, crystallized for 5 min at 120°C with ϕ_c = 0.13 [Fig.

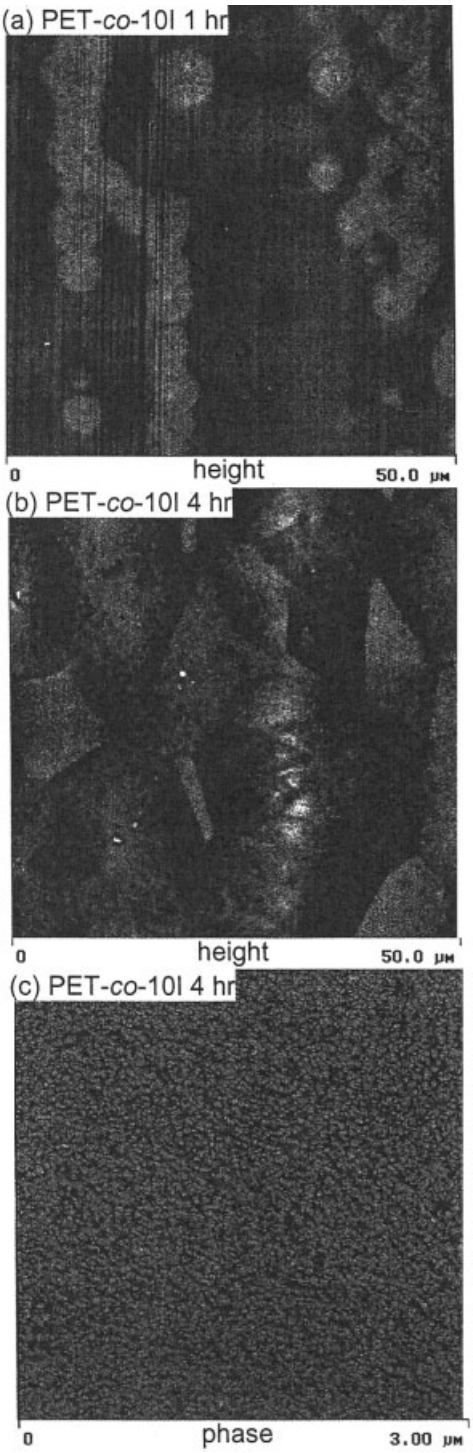

Figure 8 AFM images of PET-*co*-10I cold crystallized at 120°C: (a) height image after crystallization for 1 h; (b) height image after crystallization for 4 h; and (c) high-resolution phase image from a spherulite arm in (b).

9(a)]. The spherulite diameter was about 1.2 μm. It seemed that the unusually high crystallization rate of blocky copolymers was at least partially the result of an enhanced rate of spherulite nucleation, perhaps attributable to the presence of PEI blocks. After 4 h at 120°C, the coarse 1.2- to 1.8-μm spherulites were almost entirely space filling, although the spherulites did not have sharp boundaries and some featureless nonspherulitic regions remained even after long crystallization times [Fig. 9(b)].

All the blocky copolymers crystallized as loosely organized spherulites, as seen in the 3-μm AFM images in Figure 9(c–h). Possibly, spherulites of PET-*b*-20I and PET-*b*-30I were even more loosely organized than those of PET-*b*-10I. The small embryonic spherulites consisted of short lamellae about 35 nm thick radiating from a central nucleus. No clear boundaries separated the radiating lamellae of the small spherulites from the unorganized granular lamellae of the nonspherulitic regions. A resemblance to morphological features described by Keith and Padden[29–31] and others[32–36] suggested that less-crystallizable PEI blocks were rejected from the crystals into the interlamellar regions. Although the possibility existed that the PET unit cell accommodated PEI blocks to some extent, the compelling morphological observations indicated that the PEI blocks were mainly rejected from the crystals.

Oxygen transport

Typical experimental curves in Figure 10 describe the oxygen flux $J(t)$ through films of cold-crystallized PET, PET-*co*-10I, and PET-*b*-10I. The flux curves were normalized to a film thickness of 200 μm to facilitate comparisons among specimens that varied somewhat in thickness. Crystallization affected both the nonsteady-state and steady-state parts of the oxygen–flux curve. The nonsteady-state region broadened (slower diffusion) and the flux decreased (lower permeability).

To obtain the diffusivity D and to accurately determine the permeability P, oxygen flux for a film of thickness l was fit to the solution of Fick's second law

$$J(t) = \frac{Pp}{l}\left[1 + 2\sum_{n=1}^{\infty}(-1)^n \exp\left(-\frac{D\pi^2 n^2 t}{l^2}\right)\right] \quad (4)$$

with appropriate boundary conditions.[4] The fit to the solution of Fick's second law is included with the experimental points in Figure 10. The two fitting parameters P/l and D/l^2 were used to obtain diffusivity D and to accurately determine the permeability P. Solubility S was calculated from the relationship $S = PD^{-1}$.

Before crystallization, PEI had much lower oxygen permeability than that of PET, 0.090 compared to 0.424 cc(STP) cm m^{-2} atm^{-1} day^{-1} (Table III). Incorporation of isophthalate into PET, as either a random copolymer or a blocky copolymer, decreased the permeability according to the logarithmic additive relationship described previously.[37] The effect of cold crystallization on oxygen barrier properties is shown in Figure 11 with volume crystallinity ϕ_c, calculated from

$$\phi_c = \frac{\Delta H}{\Delta H^\circ}\frac{\rho}{\rho_c} \quad (5)$$

where ΔH is obtained from the DSC heating scan, ΔH° is the heat of melting of the perfect crystal taken as 125 J g^{-1},[38] ρ is the measured density, and ρ_c is the crystal density. Although ϕ_c is not very sensitive to ρ_c in eq. (5), ρ_c is taken as 1.515 g cm^{-3} for PET[19] and as 1.476 g cm^{-3} for imperfect crystals of PET-*co*-10I and the blocky copolymers.

Crystallization substantially decreased oxygen permeability. The highest crystallinity achieved with PET decreased P by a factor of 2.1, from 0.424 to about 0.202 cc(STP) cm m^{-2} atm^{-1} day^{-1} (Table III), attributed almost entirely to a decrease in D. Crystallinity reduced P of PET-*co*-10I by the same factor of 2.1, from 0.370 to 0.180 cc(STP) cm m^{-2} atm^{-1} day^{-1}, and reduced P of the blocky copolymers by a factor of 2.2–2.3. Reduced P of all the copolymers was the result of decreases in both D and S. A feature that differentiated the copolymers from PET was the effect of crystallinity on S. Whereas S of PET was almost independent of crystallinity, S of the copolymers deceased linearly with ϕ_c and extrapolated to $S = 0$ at $\phi_c = 1$, as indicated by the solid lines in Figure 11.

The temperature dependency of P and D was determined for crystallized films of PET, PET-*co*-10I, and PET-*b*-10I of high crystallinity. An Arrhenius relationship was exhibited, and the resulting activation energies for oxygen permeation E_P and diffusion E_D are presented in Table IV. Activation energies for amorphous PET from the literature are included for comparison.[39] With crystallization, E_P decreased slightly, whereas E_D was essentially unaffected.

DISCUSSION

Oxygen sorption

Gas-transport behavior of a crystalline polymer is often considered in terms of a two-phase model, consisting of an impermeable crystalline phase dispersed in a permeable amorphous matrix. Thus, both sorption and diffusion are seen as taking place in the amorphous phase. The resulting relationship between solubility and volume crystallinity is

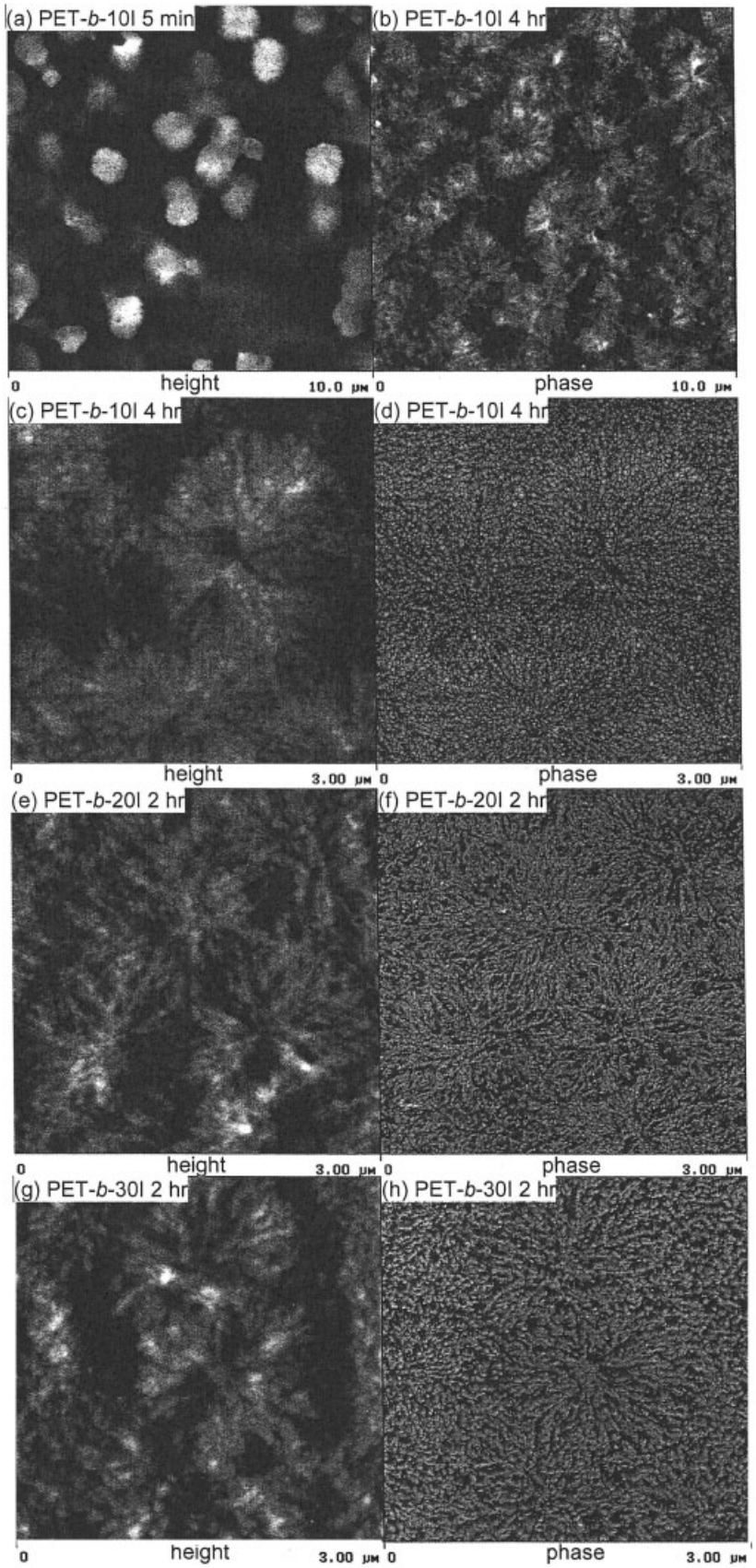

Figure 9 AFM images of blocky copolymers crystallized at 120°C: (a) height image of PET-*b*-10I after crystallization for 5 min; (b) height image of PET-*b*-10I after crystallization for 4 h; (c) high-resolution height image from a spherulite in (b); (d) corresponding phase image of (c); (e) high-resolution height image of PET-*b*-20I after crystallization for 2 h; (f) corresponding phase image of (e); (g) high-resolution height image of PET-*b*-30I after crystallization for 2 h; (h) corresponding phase image of (g).

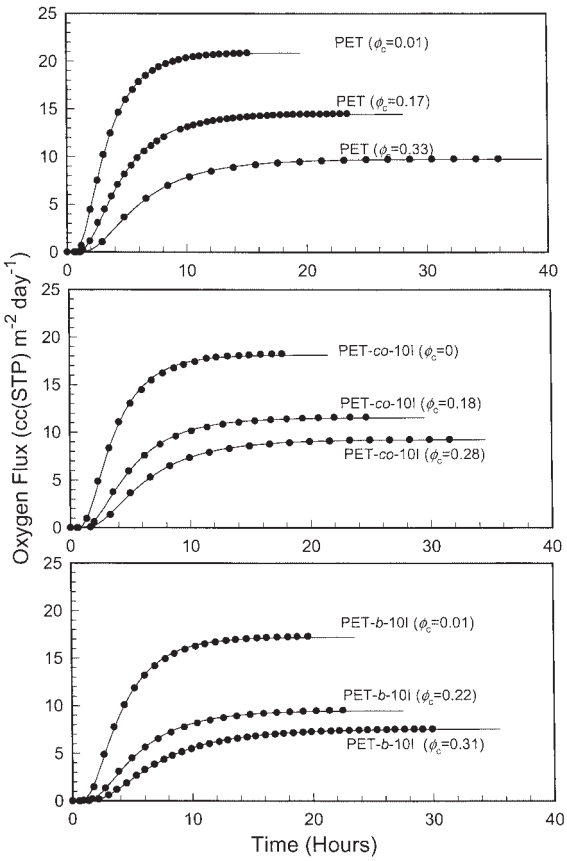

Figure 10 Experimental oxygen flux data and the fit to eq. (4): (a) PET; (b) PET-*co*-10I; and (c) PET-*b*-10I.

$$S = S_a(1 - \phi_c) \tag{6}$$

where S_a is the solubility of the gas in the amorphous phase. If S_a is independent of the amount of the crystallinity and equal to the solubility of the completely amorphous polymer, S will decrease linearly with volume crystallinity ϕ_c and extrapolate to zero at $\phi_c = 1$. This behavior is observed for PET-*co*-10I and the blocky copolymers (Fig. 11). However, in some cases [e.g., PET[4–6] and polyethylene naphthalate (PEN)[3]] S_a is found to increase with crystallinity as a result of decreasing density of the amorphous phase. Increasing S_a essentially offsets increasing ϕ_c in eq. (6) so that bulk solubility of PET is virtually independent of crystallinity.

Following the approach used previously,[3] analysis of PET oxygen solubility was carried out with a modified two-phase model with constant crystalline phase density ρ_c and variable amorphous phase density $\rho_a(\rho)$. For bulk density ρ, ρ_a is obtained from the expression

$$\rho = \rho_c\phi_c + \rho_a(1 - \phi_c) \tag{7}$$

with volume crystallinity ϕ_c determined from eq. (5).

A linear relationship between S_a and $\nu_a = \rho_a^{-1}$ at 25°C and 1 atm was previously reported for crystallized PET[4,5] and PEN[3]; for glassy copolymers of PET[37,40]; and for cold-drawn PEN, PET, and a PET copolymer.[41] The linear relationship appears to be a common characteristic of polyesters of ethylene glycol and aromatic diacids. The general correlation between S_a and ν_0 is expressed as

$$S_a = \beta(\nu_a - \nu_0) \tag{8}$$

where ν_0 is the specific volume at zero solubility. According to free volume concepts that view sorption as the process of filling holes of static free volume, the quantity $(\nu_a - \nu_0)$ identifies the excess-hole free volume available to oxygen.[37,41] Orientation of the glassy state decreases the excess-hole free volume, whereas crystallization often has the effect of increasing the excess-hole free volume of the amorphous phase. The extrapolated quantity ν_0 is not necessarily the same for all polyesters and reflects a characteristic of the particular chemical structure. However, the slope β is about 3.6 cc(STP) g cm^{-6} atm^{-1} for all the aromatic polyesters studied. The slope reflects the density of sorbed oxygen,[37] and constant β indicates fundamental similarity in the characteristics of the accessible free volume in the amorphous phase.

Testing the relationship between S_a and ν_a for PET requires reliable values of ρ_a. The key is the choice of ρ_c in eq. (7). A density of 1.476 g cm^{-3} is thought to be appropriate for the defective PET crystals obtained by strain-induced crystallization and by cold crystallization of PET copolymers.[27] It is possible that cold crystallization of PET at lower temperatures also produces defective crystals.[5] However, results using a ρ_c value of 1.476 g cm^{-3} lay considerably above the correlation previously obtained for oriented glassy PET,[41] and resulted in values of ν_0 and β that were inconsistent with established characteristics of aromatic polyesters. The crystal density of the PET triclinic unit cell of 1.515 g cm^{-3} may be more appropriate,[6] and the relationship between S_a and ν_a using this value of ρ_c is plotted in Figure 12. Results for crystalline PET are described satisfactorily by the correlation for oriented glassy PET, which is indicated by the dashed line. Correlation in Figure 12 implies that accessible free volume in the amorphous phase of crystalline PET is not fundamentally different from accessible free volume in oriented PET and in aromatic polyesters generally. The values of ρ_a and S_a are tabulated in Table III.

A plot of amorphous density ρ_a as a function of bulk density ρ shows the strong tendency of PET to densify during crystallization (Fig. 13). A previous study reported amorphous phase densification of cold-crystallized PET based on X-ray diffraction methods.[27] Comparison with results from oxygen solubility shows the identical decrease in ρ_a at lower levels of

TABLE III
Oxygen Barrier Properties of Films Crystallized at 120°C[a]

Polymer	ρ (g cm^{-3})	ΔH (J g^{-1})	ϕ_c	P	D	S	ρ_a (g cm^{-3})	S_a
PET								
Quenched	1.3364 ± 0.0004	1	0.01	0.424 ± 0.004	5.0 ± 0.1	0.098 ± 0.001	1.335	0.099
10 min	1.3412 ± 0.0007	5	0.04	0.401 ± 0.009	4.8 ± 0.2	0.097 ± 0.002	1.335	0.100
15 min	1.3447 ± 0.0008	9	0.06	0.373 ± 0.013	4.5 ± 0.1	0.096 ± 0.001	1.333	0.102
20 min	1.3609 ± 0.0013	24	0.17	0.306 ± 0.018	3.8 ± 0.3	0.093 ± 0.001	1.329	0.113
40 min	1.3802 ± 0.0015	41	0.30	0.232 ± 0.006	3.0 ± 0.1	0.090 ± 0.001	1.323	0.128
2 h	1.3823 ± 0.0012	43	0.31	0.218 ± 0.006	2.9 ± 0.2	0.087 ± 0.003	1.322	0.127
4 h	1.3848 ± 0.0010	45	0.33	0.202 ± 0.003	2.7 ± 0.1	0.087 ± 0.003	1.321	0.129
PET-*co*-10I								
Quenched	1.3405 ± 0.0006	0	0.00	0.371 ± 0.004	4.5 ± 0.1	0.095 ± 0.001	1.341	0.095
15 min	1.3415 ± 0.0010	3	0.02	0.364 ± 0.006	4.3 ± 0.2	0.095 ± 0.002	1.339	0.097
30 min	1.3460 ± 0.0017	7	0.05	0.323 ± 0.004	4.1 ± 0.1	0.091 ± 0.001	1.339	0.096
1 h	1.3657 ± 0.0038	24	0.18	0.243 ± 0.009	3.5 ± 0.1	0.080 ± 0.003	1.342	0.098
4 h	1.3777 ± 0.0010	36	0.25	0.202 ± 0.001	3.1 ± 0.1	0.075 ± 0.003	1.342	0.103
8 h	1.3814 ± 0.0005	38	0.28	0.180 ± 0.001	2.9 ± 0.1	0.072 ± 0.001	1.344	0.100
PET-*b*-10I								
Quenched	1.3399 ± 0.0002	1	0.01	0.350 ± 0.004	4.2 ± 0.1	0.096 ± 0.003	1.339	0.097
4 min	1.3440 ± 0.0010	6	0.04	0.315 ± 0.001	4.0 ± 0.1	0.091 ± 0.001	1.338	0.095
5 min	1.3571 ± 0.0019	18	0.13	0.258 ± 0.008	3.6 ± 0.1	0.083 ± 0.003	1.339	0.096
6 min	1.3723 ± 0.0009	30	0.22	0.194 ± 0.003	3.1 ± 0.1	0.072 ± 0.002	1.343	0.093
10 min	1.3776 ± 0.0003	35	0.26	0.174 ± 0.004	2.9 ± 0.1	0.069 ± 0.002	1.341	0.094
30 min	1.3806 ± 0.0010	40	0.30	0.155 ± 0.001	2.6 ± 0.1	0.069 ± 0.001	1.340	0.098
1 h	1.3820 ± 0.0008	41	0.31	0.154 ± 0.001	2.6 ± 0.1	0.069 ± 0.001	1.340	0.099
4 h	1.3829 ± 0.0009	41	0.31	0.149 ± 0.001	2.5 ± 0.1	0.069 ± 0.001	1.342	0.100
PET-*b*-20I								
Quenched	1.3406 ± 0.0005	1	0.01	0.278 ± 0.004	3.8 ± 0.1	0.085 ± 0.002	1.340	0.085
4 h	1.3817 ± 0.0008	39	0.29	0.125 ± 0.002	2.4 ± 0.1	0.060 ± 0.001	1.343	0.085
PET-*b*-30I								
Quenched	1.3429 ± 0.0004	1	0.01	0.239 ± 0.006	3.4 ± 0.1	0.081 ± 0.003	1.342	0.082
4 h	1.3817 ± 0.0006	38	0.28	0.111 ± 0.003	2.2 ± 0.1	0.058 ± 0.001	1.344	0.082
PEI								
Quenched	1.3464 ± 0.0003	0	0	0.090 ± 0.003	1.7 ± 0.1	0.061 ± 0.002	—	—

[a] P, cc(STP) cm m^{-2} atm^{-1} day^{-1}; D, $\times 10^{-13}$ m^2 s^{-1}; S and S_a, cc(STP) cm^{-3} atm^{-1}.

crystallinity; however, solubility results suggest that ρ_a continues to decrease smoothly at higher crystallinity, whereas X-ray results suggest a sharper drop (Fig. 13). The difference is attributed to the higher crystallization temperatures used in the X-ray study. Dedensification of PEN, as determined by the oxygen solubility method,[3] is also included in Figure 13 for comparison. Although the effect appears to be more dramatic for PEN than for PET, it should be noted that the density difference between amorphous glass and crystal is smaller for PEN than for PET.

Structural model for crystalline PET

Morphologically, cold crystallization of PET proceeds by spherulite nucleation and growth until the spherulites are space filling. Following the structural model developed for PEN,[3] PET can be viewed morphologically as a dispersion of spherulites in a continuous amorphous matrix. However, the impermeable units of crystallized PET are lamellar crystals, not spherulites. The individual spherulite is itself a composite structure consisting of impermeable lamellar crystals arranged in a permeable interlamellar amorphous phase. Because of the constraint imposed by chain segments in crystals on amorphous chain segments, the interlamellar amorphous phase differs from the amorphous matrix with respect to chain conformation,[42] and to other properties as well, including density and gas permeability.[4,5]

The amorphous density ρ_a, extracted from eq. (7) and given in Table III, combines characteristics of the amorphous matrix and the interlamellar amorphous phase. The decrease in ρ_a as crystallinity increases is not interpreted as the gradual dedensification of a homogeneous amorphous phase. As volume fraction crystallinity increases the change in ρ_a averages the gradual increase in amount of dedensified interlamellar amorphous phase and corresponding decrease in amount of amorphous matrix. Similarly, S_a averages oxygen solubility in the amorphous matrix and in the dedensified interlamellar regions.

For simplicity, volume crystallinity of the spherulites ϕ_s is assumed constant during spherulite growth,

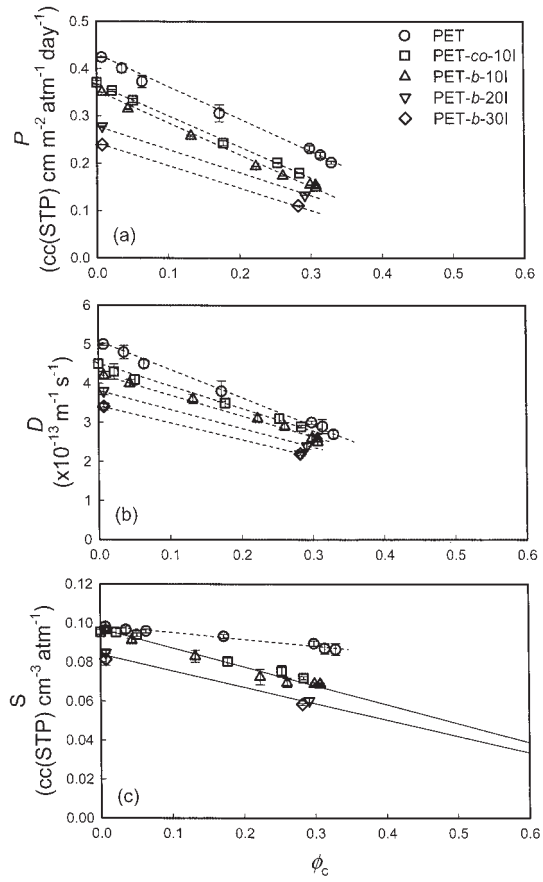

Figure 11 Effect of crystallinity on oxygen-transport parameters: (a) permeability; (b) diffusivity; and (c) solubility. The dashed lines describe the data; the solid lines extrapolate to $S = 0$ at $\phi_c = 1$.

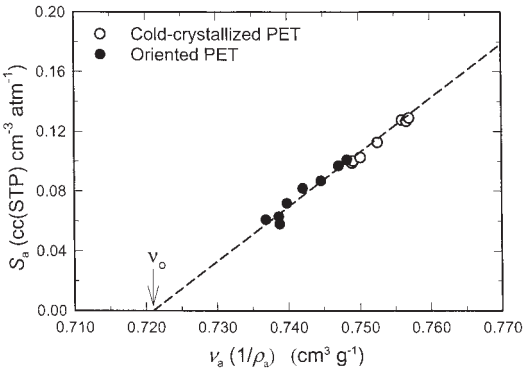

Figure 12 S_a versus ν_a for cold-crystallized PET. Data for oriented PET are taken from Liu et al.[41]

which is identified as the region of rapidly increasing ϕ_c in Figure 6. The point in Figure 6 where ϕ_c starts to level off gives $\phi_s = 0.31$ for cold crystallization at 120°C. The small increase in ϕ_c at longer times is attributed to increasing ϕ_s of space-filling spherulites because of secondary crystallization. The following discussion is limited to primary crystallization. Assuming that the density of the amorphous matrix ρ_{am} is the same as the density of amorphous PET (1.335 g cm^{-1}) and that the dedensified interlamellar amorphous phase has constant density ρ_{as}, a relationship between ρ_a from solubility and volume fraction crystallinity ϕ_c can be developed with ρ_{as} as the only unknown

$$\rho_a = \rho_{am} - \frac{\phi_c}{1 - \phi_c}\left(\frac{1 - \phi_s}{\phi_s}\right)(\rho_{am} - \rho_{as}) \qquad (9)$$

where ϕ_{as} is the volume fraction of interlamellar amorphous phase. A linear relationship between ρ_a and the quantity $\phi_c(1 - \phi_c)^{-1}$ in Figure 14 indicates that a constant value of ρ_{as}, independent of the amount of crystallinity, satisfactorily describes the change in amorphous density of crystallized PET. A value of $\phi_s = 0.31$ results in ρ_{as} of 1.321 g cm^{-3} for cold crystallization at 120°C, which is close to the experimental value (Table III). Secondary crystallization increases ϕ_s, which can impart further constraint and dedensification of the interlamellar amorphous phase. Nevertheless, the effect of secondary crystallization is negligible. Data for PEN are also plotted according to eq. (9) in Figure 14. Based on crystallinity, the tendency to dedensify is only slightly stronger for PEN than it is for PET.

The structural model for permeation with three phases of constant density constitutes a refinement of the two-phase model with impermeable crystalline phase and permeable amorphous phase of variable density. By combining eq. (7) with eq. (9), the amorphous density is given as

TABLE IV
Activation Energies for Oxygen Permeation and Diffusion

Polymer	Density (g cm^{-3})	ϕ_c	E_P (kJ mol^{-1})	E_D (kJ mol^{-1})
Quenched PET[a]	1.337	0.01	29.0	39.7
Crystallized PET, 120°C, 4 h	1.3848	0.33	25.9	38.9
Crystallized PET-*co*-10I, 120°C, 8 h	1.3804	0.28	26.5	38.6
Crystallized PET-*b*-10I, 120°C, 4 h	1.3826	0.31	26.0	41.2

[a] Data from Hu et al.[39]

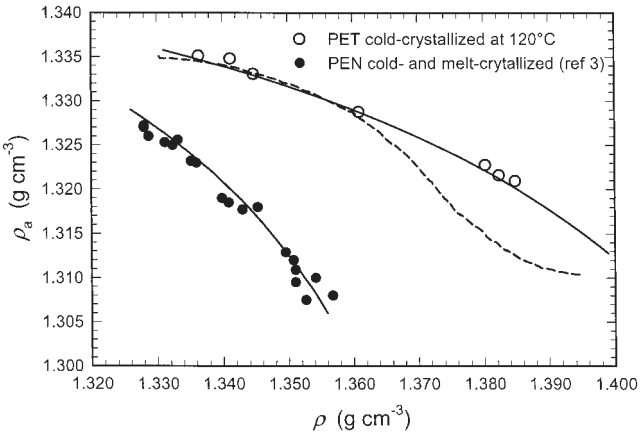

Figure 13 Amorphous density plotted versus bulk density for cold-crystallized and melt-crystallized PET. The solid curve is from eq. (10). The dashed curve is a fit to data for PET presented in Bornschlegl and Bonart.[27] Data for PEN are taken from Hu et al.[3]

$$\rho_a = \frac{\rho_{am} - \rho\chi}{1 - \chi} \tag{10}$$

where

$$\chi = \left(\frac{1 - \phi_s}{\phi_s}\right)\left(\frac{\rho_{am} - \rho_{as}}{\rho_c - \rho}\right) \tag{11}$$

Using values given above for spherulite crystallinity ϕ_s and phase densities ρ_{am}, ρ_{as}, and ρ_c of PET, and the appropriate values for PEN from the literature,[3] the results from eq. (10) are represented in Figure 13 as solid curves.

In contrast to PET and PEN, oxygen solubility of cold-crystallized copolymers with isophthalate conforms to the simple two-phase solubility model with constant crystalline and amorphous phase densities.

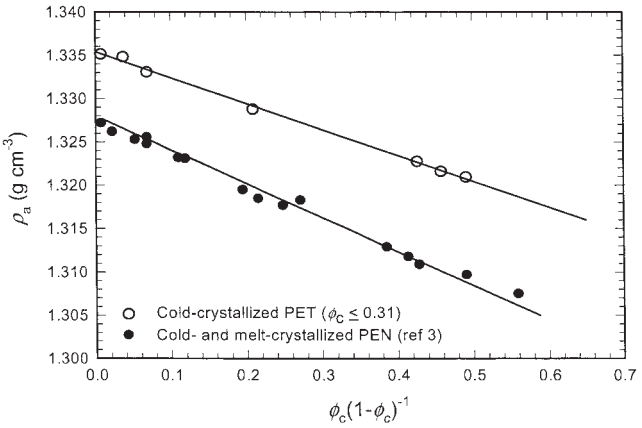

Figure 14 Relationship between amorphous phase density and crystallinity of PET plotted according to the three-phase model [eq. (9)]. Data for PEN are taken from Hu et al.[3]

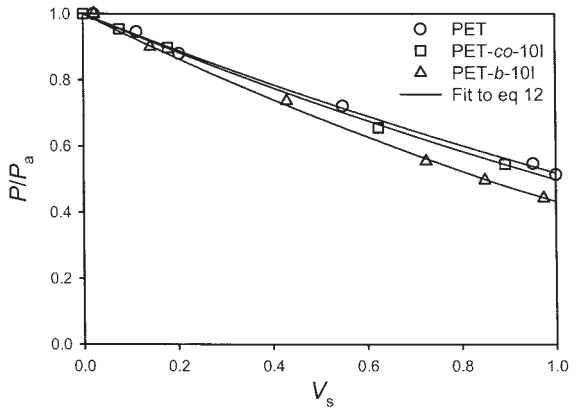

Figure 15 Relative permeability plotted versus V_s and the fit to the Maxwell model [eq. (12)]. For PET, P_s = 0.220 and P_a = 0.424 cc(STP) cm m^{-2} atm^{-1} day^{-1}; for PET-*co*-10I, P_s = 0.188 and P_a = 0.371 cc(STP) cm m^{-2} atm^{-1}; for PET-*b*-10I, P_s = 0.150 and P_a = 0.350 cc(STP) cm m^{-2} atm^{-1}.

Copolymerization apparently prevents dedensification of interlamellar amorphous regions so that $\rho_{as} = \rho_a$. It may be that segregation of kinked isophthalate units to the amorphous regions relieves constraint on the interlamellar amorphous chain segments. Point by point values of ρ_a and S_a, taken from eqs. (6) and (7) for cold-crystallized copolymers, are entered in Table III.

Structural model for permeability

By considering crystallized PET as a dispersion of less-permeable spherulites in a more permeable amorphous matrix, the Maxwell equation can be used to describe oxygen permeability. Assuming constant volume crystallinity of spherulites ϕ_s during spherulite growth, increasing bulk volume crystallinity ϕ_c increases the volume fraction occupied by spherulites as $V_s = \phi_c/\phi_s$. When the spherulites are space filling, V_s is equal to unity and $\phi_s = \phi_c$. If it is further assumed that permeability of the spherulites P_s is constant and does not change with V_s, and permeability of the amorphous matrix P_a is equal to the permeability of amorphous PET of 0.424 cc(STP) cm m^{-2} atm^{-1} day^{-1}, the Maxwell equation for a spherical dispersion takes the form[3]

$$P = P_a\left\{1 + \frac{3V_s}{\left[\frac{(P_s/P_a) + 2}{(P_s/P_a) - 1}\right] - V_s}\right\} \tag{12}$$

with P_s as the only unknown. Although initially developed for a dilute dispersion of spheres, eq. (12) has been shown to be valid over the entire composition range.[43] The quantity P/P_a is plotted versus V_s in Figure 15 for crystallized PET in the primary crystallization region where $\phi_c \leq \phi_s$. The solid line is the fit

TABLE V
Physical Properties of Spherulites[a]

Polymer	ρ_{as} (g cm^{-3})	P_{as}	S_{as}	D_{as}	ϕ_s	ρ_s (g cm^{-3})	P_s	S_s	D_s	α
PET	1.321	0.607	0.130	5.4	0.31	1.381	0.220	0.090	2.8	12
PET-*co*-10I	1.341	0.371	0.095	4.5	0.28	1.379	0.188	0.068	3.2	10
PET-*b*-10I	1.340	0.350	0.096	4.2	0.31	1.382	0.150	0.066	2.6	11

[a] P_{as} and P_s, cc(STP) cm m^{-2} atm^{-1} day^{-1}; D_{as} and D_s, $\times 10^{-13}$ m^2 s^{-1}; S_{as} and S_s, cc(STP) cm^{-3} atm^{-1}.

to eq. (12) with constant $P_s = 0.220$ cc(STP) cm m^{-2} atm^{-1} day^{-1}.

The same analysis applies to PET-*co*-10I and PET-*b*-10I, with the stipulation that the interlamellar amorphous phase does not differ from the amorphous matrix in terms of density and transport properties. The point in Figure 6 where ϕ_c starts to level off gives $\phi_s = 0.28$ for PET-*co*-10I and $\phi_s = 0.31$ for PET-*b*-10I. Taking P_a as 0.371 and 0.350 cc(STP) cm m^{-2} atm^{-1} day^{-1} for PET-*co*-10I and PET-*b*-10I, respectively, the experimental results and the solid line fits to eq. (12) are included in Figure 15. Equation (12) satisfactorily describes the data with constant P_s values of 0.188 and 0.150 cc(STP) cm m^{-2} atm^{-1} day^{-1} for PET-*co*-10I and PET-*b*-10I, respectively. The lower P_s value of PET-*b*-10I compared to that of PET-*co*-10I arises from higher ϕ_s and lower P_a.

The impermeable structural element of the spherulite is the lamellar crystal. Structurally, spherulites resemble the dispersion of impermeable platelets of given aspect ratio that has been modeled by Cussler et al.[44–47] For isotropic, space-filling spherulites, where the lamellae (platelets) are randomly oriented, the permeability of the spherulite is expressed as[3]

$$P_s = P_{as}\left[1 + \frac{\alpha^2\phi_s^2}{12(1-\phi_s)}\right]^{-1} \qquad (13)$$

where P_s is the permeability of the spherulite, $P_{as} = D_{as}S_{as}$ refers to the permeability of the interlamellar amorphous regions of the spherulite, ϕ_s is the volume crystallinity of the spherulite, and α is the aspect ratio of the lamellae defined as length divided by width.

Interlamellar amorphous regions of the PET spherulite with density ρ_{as} of 1.321 g cm^{-3} have oxygen solubility S_{as} of 0.130 cc(STP) cm^{-3} from Figure 12. Diffusivity of oxygen in the interlamellar amorphous regions D_{as} is obtained from the relationship between diffusivity and fractional free volume,[3] with data from the previous study,[41] and is 5.4×10^{-13} m^2 s^{-1} for crystallized PET. The resulting α of the impermeable lamellar crystals is 12 for PET (Table V). The same analysis applies to the copolymers with the stipulation that the interlamellar amorphous phase does not differ from the amorphous matrix in terms of density and transport properties. The results are $\alpha = 10$ for PET-*co*-10I and $\alpha = 11$ for PET-*b*-10I (Table V). It seems reasonable that PET crystals have the best order with the highest α and the statistical copolymer crystals are the most defective with the lowest α.

CONCLUSIONS

This study compares crystallization of random and blocky copolymers in which up to 30% of the terephthalate in PET is replaced with isophthalate. Comonomer distribution strongly affects the kinetics of isothermal crystallization. Blocky copolymers crystallize more rapidly than PET, at least in part, as the result of enhanced spherulite nucleation. Statistical distribution of isophthalate retards crystallization, although statistical copolymers with 10 and 20% isophthalate ultimately achieve almost the same level of crystallinity as that of the blocky copolymers. Whereas PET and a statistical copolymer with 10% isophthalate crystallize as space-filling spherulites with sharp boundaries, the blocky copolymers crystallize as small embryonic spherulites with no clear boundaries separating the radiating lamellae from the unorganized granular lamellae of nonspherulitic regions. These features suggest rejection of a less-crystallizable component into the interlamellar regions. However, from the high level of crystallinity achieved with both random and blocky copolymers, it appears that some isophthalate is incorporated into the PET crystal structure.

Crystallization significantly reduces the oxygen permeability. Decreased permeability of crystallized PET is attributed to decreasing diffusivity only, whereas decreased permeability of the copolymers arises from decreases in both diffusivity and solubility. Morphological observations provide the basis for a two-phase structural model for oxygen transport that considers a dispersion of lower-permeability spherulites in an amorphous matrix of higher permeability. The spherulites themselves are composites of impermeable crystallites and permeable interlamellar amorphous regions. In the case of PET, the interlamellar amorphous regions have lower density than that of the amorphous matrix as a result of the constrained nature of amorphous chain segments attached to crystallites; in this feature, PET resembles PEN. Increased oxygen solubility of the interlamellar amorphous re-

gions essentially offsets the decrease from impermeable crystallites, resulting in oxygen solubility that appears to be independent of crystallinity. In contrast, copolymerization with isophthalate prevents dedensification of the interlamellar amorphous regions. As a result, crystallization is more effective in reducing the oxygen permeability. It is speculated that segregation of kinked isophthalate units to the amorphous regions of the spherulite relieves constraint on the interlamellar amorphous chain segments.

This research was generously supported by KoSa. Support from Modern Controls, Inc. for development of a facility for gas-transport studies at Case Western Reserve University is gratefully acknowledged.

References

1. Liu, R. Y. F.; Hu, Y. S.; Hibbs, M. R.; Collard, D. M.; Schiraldi, D. A.; Hiltner, A.; Baer, E. J Appl Polym Sci, to appear.
2. Hiltner, A.; Liu, R. Y. F.; Hu, Y. S.; Baer, E. J Polym Sci Part B: Polym Phys 2005, 43, 1047.
3. Hu, Y. S.; Liu, R. Y. F.; Zhang, L. Q.; Rogunova, M.; Schiraldi, D. A.; Nazarenko, S.; Hiltner, A.; Baer, E. Macromolecules 2002, 35, 7326.
4. Sekelik, D. J.; Stepanov, S. V.; Nazarenko, S.; Schiraldi, D.; Hiltner, A.; Baer, E. J Polym Sci Part B: Polym Phys 1999, 37, 847.
5. Polyakova, A.; Stepanov, E. V.; Sekelik, D.; Schiraldi, D. A.; Hiltner, A.; Baer, E. J Polym Sci Part B: Polym Phys 2001, 39, 1911.
6. Lin, J.; Shenogin, S.; Nazarenko, S. Polymer 2002, 43, 4733.
7. Hu, Y. S.; Rogunova, M.; Schiraldi, D. A.; Hiltner, A.; Baer, E. J Appl Polym Sci 2002, 86, 98.
8. Joseph, E.; Wilkes, G. L.; Baird, D. G. Polymer 1985, 26, 689.
9. Olley, R. H.; Bassett D. C.; Blundell, D. L. Polymer 1986, 27, 344.
10. Rasburn, J.; Hine, P. J.; Ward, I. M.; Olley, R. H.; Bassett, D. C.; Kabeel, M. A. J Mater Sci 1995, 30, 615.
11. Shabana, H. M.; Olley, R. H.; Bassett, D. C.; Zachmann, H. G. J. Macromol Sci Phys 1996, B35, 691.
12. Karayannidis, G. P.; Sideridou, I. D.; Zamboulis, D. N.; Bikiaris, D. N.; Sakalis, A. J. J Appl Polym Sci 2000, 78, 200.
13. Lee, S. W.; Ree, M.; Park, C. E.; Jung, Y. K.; Park, C.-S.; Jin, Y. S.; Bae, D. C. Polymer 1999, 40, 7137.
14. Kint, D. P. R.; De Ilarduya, A. M.; Sansalvadló, A.; Ferrer, J.; Muñoz-Guerra, S. J Appl Polym Sci 2003, 90, 3076.
15. Jabarin, S. A. J Appl Polym Sci 1987, 34, 103.
16. Bicerano, J. J Mater Sci Rev Macromol Chem Phys 1998, C38, 391.
17. Keller, A. In Polymers, Liquid Crystals and Low-Dimensional Solids, March, N.; Tosi, M., Eds.; Plenum Press: New York, 1984; Chapter 2.
18. Li, B.; Yu, J.; Lee, S.; Ree, M. Polymer 1999, 40, 5371.
19. Fakirov, S.; Fischer, E. W.; Schmidt, G. F. Makromol Chem 1975, 176, 2459.
20. Yamadera, R.; Sonoda, C. J Polym Sci Polym Lett 1965, 3, 411.
21. Kobayashi, S.; Hachiboshi, M. Rep Prog Polym Phys Jpn 1970, 13, 157.
22. Kobayashi, S.; Hachiboshi, M. Rep Prog Polym Phys Jpn 1970, 13, 161.
23. Hachiboshi, M.; Fukada, T.; Kobayashi, S. J. Macromol Sci Phys 1969, B3, 525.
24. Fischer, von E. W. Prog Colloid Polym Sci 1975, 57, 149.
25. Berghmans, H.; Govaerts, F.; Overbergh, N. J Polym Sci Polym Phys Ed 1979, 17, 1251.
26. Zhang, Y.; Gu, L. Eur Polym J 2000, 36, 759.
27. Bornschlegl, E.; Bonart, R. Colloid Polym Sci 1980, 258, 319.
28. Groeninckx, G.; Reynaers, H.; Berghmans, H.; Smets, G. J Polym Sci Polym Phys Ed 1980, 18, 1311.
29. Keith, H. D.; Padden, F. J., Jr. J Appl Phys 1963, 34, 2409.
30. Keith, H. D.; Padden, F. J., Jr. J Appl Phys 1964, 35, 1270.
31. Keith, H. D.; Padden, F. J., Jr. J Appl Phys 1964, 35, 1286.
32. Hudson, S. D.; Davis, D. D.; Lovinger, A. J. Macromolecules 1992, 25, 1759.
33. Hsiao, B. S.; Sauer, B. B. J Polym Sci Part B: Polym Phys 1993, 31, 901.
34. Debier, D.; Jonas, A. M.; Legras, R. J Polym Sci Part B: Polym Phys 1998, 36, 2197.
35. Jonas, A. M.; Ivanov, D. A.; Yoon, D. Y. Macromolecules 1998, 31, 5352.
36. Wu, L.; Lisowski, M.; Talibuddin, S.; Runt, J. Macromolecules 1999, 32, 1576.
37. Polyakova, A.; Liu, R. Y. F.; Schiraldi, D. A.; Hiltner, A.; Baer, E. J Polym Sci Part B: Polym Phys 2001, 39, 1889.
38. Wunderlich, B. Macromolecular Physics, Vol. 1; Academic Press: New York, 1973; p 389.
39. Hu, Y. S.; Liu, R. Y. F.; Schiraldi, D. A.; Hiltner, A.; Baer, E. Macromolecules 2004, 37, 2136.
40. Polyakova, A.; Connor, D. M.; Collard, D. M.; Schiraldi, D. A.; Hiltner, A.; Baer, E. J Polym Sci Part B: Polym Phys 2001, 39, 1900.
41. Liu, R. Y. F.; Schiraldi, D. A.; Hiltner, A.; Baer, E. J Polym Sci Part B: Polym Phys 2002, 40, 862.
42. Ivanov, D. A.; Pop, T.; Yoon, D. Y.; Jonas, A. M. Macromolecules 2002, 35, 9813.
43. Petropoulos, J. H. J Polym Sci Polym Phys Ed 1985, 23, 1309.
44. Cussler, E. L.; Hughes, S. E.; Ward, W. J., III; Aris, R. J Membr Sci 1988, 38, 161.
45. Eitzman, D. M.; Melkote, R. R.; Cussler, E. L. AIChE J 1996, 42, 2.
46. Falla, W. R.; Mulski, M.; Cussler, E. L. J Membr Sci 1996, 119, 129.
47. Hu, Y. S.; Liu, R. Y. F.; Hiltner, A.; Baer, E. J Polym Sci Part B: Polym Phys 2002, 40, 2489.